PNAS RESEARCH ARTICLE | NEUROSCIENCE OPEN ACCESS

Intranasal delivery of full-length anti-Nogo-A antibody: A potential alternative route for therapeutic antibodies to central nervous system targets

Daphne Correa[a,b,1,2], Myriam I. Scheuber[b], Huimin Shan[b], Oliver W. Weinmann[b], Yves A. Baumgartner[a,c], Aliona Harten[d,e,3], Anna-Sophia Wahl[f,g,h,4], Kirstin L. Skaar[b], and Martin E. Schwab[a,b,1,5]

Edited by Lawrence Steinman, Stanford University, Stanford, CA; received January 6, 2022; accepted October 3, 2022

Antibody delivery to the CNS remains a huge hurdle for the clinical application of antibodies targeting a CNS antigen. The blood–brain barrier and blood–CSF barrier restrict access of therapeutic antibodies to their CNS targets in a major way. The very high amounts of therapeutic antibodies that are administered systemically in recent clinical trials to reach CNS targets are barely viable cost-wise for broad, routine applications. Though global CNS delivery of antibodies can be achieved by intrathecal application, these procedures are invasive. A non-invasive method to bring antibodies into the CNS reliably and reproducibly remains an important unmet need in neurology. In the present study, we show that intranasal application of a mouse monoclonal antibody against the neurite growth-inhibiting and plasticity-restricting membrane protein Nogo-A leads to a rapid transfer of significant amounts of antibody to the brain and spinal cord in intact adult rats. Daily intranasal application for 2 wk of anti-Nogo-A antibody enhanced growth and compensatory sprouting of corticofugal projections and functional recovery in rats after large unilateral cortical strokes. These findings are a starting point for clinical translation for a less invasive route of application of therapeutic antibodies to CNS targets for many neurological indications.

intranasal | stroke recovery | neurodegeneration | antibody therapy | Nogo-A

Therapeutic antibodies against central nervous system (CNS) targets are currently making their way into the clinic, e.g., for neurodegenerative diseases such as Alzheimer's or Parkinson's disease, for multiple sclerosis, or spinal cord injury (1–6). An important problem remains the access of antibodies to the CNS: Only around 0.1% of the amount of systemically administered therapeutic antibodies reach the CNS (7). This is due to the presence of two barrier systems, the blood–brain barrier (BBB) and the blood–cerebrospinal fluid barrier (8). To overcome this low bioavailability, very large doses of antibodies are often applied (9–14). Strategies such as the transient opening of the BBB via focused ultrasound techniques (15–22) are efficient in preclinical models, but also allow nonspecific serum macromolecules to enter the CNS (23, 24). An alternative route to peripheral, systemic administration is the direct intrathecal or intracerebroventricular administration (4, 25–30). The cerebrospinal fluid (CSF) circulation in the internal and external, subdural CSF spaces provide rapid distribution throughout the brain and spinal cord (30–32). However, these routes are invasive; for broader clinical applications, a less invasive approach would be preferable, especially if long-term treatments in outpatients are required.

An interesting, unconventional route of antibody application to CNS targets is the intranasal route (33–39). This route is noninvasive and bypasses the BBB. Preclinical and clinical intranasal application of small molecules (MW 10 to 30 kD), for example BDNF mimetics (40), neuropeptides (41), insulin (42) calcitonin (43) as well as scFv antibody (38) have been demonstrated. Recently, successful intranasal delivery of macromolecules such as full-length IgG (150 kDa) resulted in detectable amounts of antibody in the rodent CNS, e.g., in models of Alzheimer's disease (44, 45). Delivery of therapeutics to the CNS by the intranasal route is thought to occur via the olfactory epithelium, possibly also along the trigeminal nerve (30, 46). The exact mechanism on how an antibody reaches the CNS via the olfactory system was not elucidated until recently (37, 39, 47, 48). Intranasally applied unspecific IgGs cross the olfactory epithelium most probably by transcytosis, whereby the so-called neonatal Fc receptor (FcRn) seems to play an important role (49, 50). Passage through open tight junctions has also been discussed (47, 48, 51).

Enhancers that accelerate the penetration of larger therapeutic molecules at the nasal olfactory epithelium have also been demonstrated (37, 48). Once in the lamina propria, they reach the outer CSF compartments and enter the brain along the olfactory or trigeminal nerve fibers in the endo- and perineural spaces. IgGs are then distributed via the perivascular spaces of cerebral blood vessels from where they penetrate the CNS parenchyma (30, 37, 39, 48, 52, 53). Many mechanistic details along this transport route remain unknown, however. An additional important question is if the amounts of a therapeutic antibody reaching the CNS are sufficient to exert its full therapeutic actions.

Significance

Cerebral strokes often result in greater physical impairments from aphasia to vision problems to motor deficits leading to persistent disability. Thus, neurorestorative therapies are crucial. However, in a stroke-clinical setting, an easy, less invasive route of an antibody application is needed. An unconventional route of therapeutic application to the CNS is via the intranasal route. Intranasal application of macromolecules such as monoclonal antibodies remains unknown. Here, we assess the feasibility and tolerance of prolonged intranasal application of a therapeutic antibody in adult rats. Further, as a proof-of-concept, we show that intranasally applied therapeutic monoclonal antibody was sufficient to enhance functional recovery in a model of ischemic stroke. The findings demonstrate an effective noninvasive approach to deliver therapeutic antibodies to CNS targets.

[1]To whom correspondence may be addressed. Email: corread@student.ethz.ch or schwab@irem.uzh.ch.

[2]Present address: Department of Health Sciences and Technology, Swiss Federal Institute of Technology-Zurich CH-8092, Zurich, Switzerland.

[3]Present address: Helmholtz Center Munich, Institute of Experimental Genetics D-85764, Neuherberg, Germany.

[4]Present address: Institute of Anatomy, Ludwig-Maximilians-University, D-80336 Munich, Germany.

[5]Present address: Institute for Regenerative Medicine, University of Zurich CH-8952, Zurich, Switzerland.

This article contains supporting information online at https://www.pnas.org/lookup/suppl/doi:10.1073/pnas.2200057120/-/DCSupplemental.

Published January 17, 2023.

Here, we used intranasal application of a mouse monoclonal antibody against the neurite growth-inhibiting and plasticity-restricting membrane protein Nogo-A to study its access to the brain and spinal cord in intact adult rats, and its repair enhancing effects in rats with large cortical strokes. The intranasal application resulted in CNS tissue concentrations of the antibody approaching the range of intrathecally infused antibody. In rats, subjected to large cortical strokes, daily intranasal application of anti-Nogo-A antibody over 2 wk induced significant improvements of skilled forelimb functions and enhanced compensatory sprouting of corticospinal fibers in the cervical spinal cord and corticopontine fibers in the brainstem. These findings demonstrate the usefulness of the noninvasive, nontraumatic intranasal route for bringing therapeutic antibodies to their CNS targets in neurological diseases.

Results

CNS Tissue Penetration and Distribution of Anti-Nogo-A Antibody after Intranasal Application. A highly specific, function-blocking mouse monoclonal antibody, 11C7, directed against the Nogo-A-specific region of rat Nogo-A (54) was used. In animal models of stroke and spinal cord injury, this antibody enhanced regrowth and compensatory sprouting of functionally important fiber systems such as the corticospinal tract as well as anatomical plasticity on different levels after 2 wk of continuous intrathecal application (28, 55, 56, 57, 58, 59). Anti-Nogo-A antibody 11C7 (biotinylated for the mouse study) was applied into the nares of anesthetized adult rodents at 0.01 mg, 0.1 mg, and 1 mg/mouse in mice and at 1 mg/rat in rats.

Mouse brains were dissected 6 h or 24 h after intranasal antibody application and anti-Nogo-A antibody detection was carried out by capture Enzyme-Linked Immunosorbent Assay (ELISA) using the antigenic delta-20 fragment of Nogo-A as a bait. Detectable concentrations of anti-Nogo-A antibody were observed 6 h after single intranasal application (1 mg of antibody), with the highest levels detected in the olfactory bulbs (Fig. 1*A*). In the 24 h postapplication group, values tended to be lower than at 6 h in all CNS regions, suggesting a rapid clearance of the antibody. In mice, the distribution and uptake of intranasally applied anti-Nogo-A antibody 6 h after a single application showed a dose-dependent increase in different CNS regions (Fig. 1*B*). Interestingly, with a dose of 10 µg, the uptake and binding capacity in the olfactory bulbs 6 h after application seemed to be saturated. High levels seen in the brainstem may indicate transport via the trigeminal nerves. Of note are the signals in the cervical spinal cord as early as 6 h after intranasal application.

Considering these possible routes of transport, the olfactory bulb and brainstem in mice were further analyzed by immunohistochemistry for the detection of biotinylated mouse monoclonal antibody 6 h after single intranasal application. 6 h after intranasal application with 100 µg of biotinylated antibody, a low diffuse as well as a cellular 11C7-biotin signal was detected in the granule cell layer of the olfactory bulbs (Fig. 1 *E* and *G*), as well as in the spinal trigeminal nucleus (Fig. 1 *J* and *L*). No biotin staining was seen in the brain of untreated control animals (Fig. 1 *D*, *F*, *I*, and *K*).

In rats, animal brains were analyzed by immunohistochemistry for the detection of mouse IgG antibodies 24 h after single and 72 h after daily repeated (3×) intranasal application. 24 h after a single intranasal application of antibody 11C7 strong immunostaining for mouse antibody was detected in the olfactory bulbs, in lamina V of the motor cortex, in the corpus callosum, hippocampus, and cerebellum, and in brainstem regions (Fig. 2*A*). Background staining in the untreated brain was very low (Fig. 2*A*). Repeated application of the same dose of mouse anti-Nogo-A antibody over 3 d (3 mg/rat in total) resulted in higher labeling intensities in all regions of the CNS (Fig. 2 *A* and *B*). Interestingly, cellular labeling could be observed in many regions, e.g., pyramidal cells in the cortex and hippocampus, Purkinje cells in the cerebellum, large neurons in brainstem nuclei, but also oligodendrocytes in white matter, e.g., corpus callosum. (Fig. 2*B*). All these cell types are known to express the target antigen Nogo-A [(60), and Allen Brain Atlas]. Double labeling for endogenous Nogo-A and mouse IgG confirmed the colocalization as shown for the trapezoid nucleus (Fig. 2 *B*, *Lower Right*). The staining probably reflects cell binding of the antibody to cell surface Nogo-A as well as intracellular antibody localization following antigen binding-induced uptake. These results show that the anti-Nogo-A antibody that reached the brain from the nasal cavity in mice and rats, was able to penetrate into the brain tissue, and reaching its antigen-expressing targets where it bound and was internalized. The Olfactory bulb and trigeminal regions showed as the first CNS regions for antibody uptake, pointing to olfactory and trigeminal nerves as the primary conduits along which the intranasally applied antibody reached the CNS.

Antibodies can activate microglia, which could, in turn, contribute to the effects seen in antibody-treated brains. We, therefore, assessed acute microglial activation in the olfactory bulb and the trigeminal nucleus of rats after 24 h of single and 72 h of repeated intranasal application of antibody 11C7. No difference in local microglial activity was observed compared with the untreated corresponding brain tissue (*SI Appendix*, Fig. S1).

To assess the amounts of transported antibody in a more quantitative way and to compare intranasal with the intrathecal application, concentrations of anti-Nogo-A or control antibody in different parts of the CNS were determined by ELISA either 7 d after daily intranasal application or after 7 d of continuous intrathecal pump infusion into the lumbar CSF space. Continuous lumbar intrathecal infusion generated a tissue gradient along the spinal cord, and significant amounts of antibodies were present also in the brainstem, cerebellum, and cortex (Fig. 3*A*). Anti-Nogo-A antibody values were consistently higher than those of the unspecific control antibody, probably by binding to Nogo-A in the tissue. A bulk of the antibodies was found in the peripheral circulation (about 1.5 mg of the infused 3 mg) at day 7 (Fig. 3*B*), in line with the known short half-life of antibodies in the CNS compartment (61). Levels for the anti-Nogo-A antibody in the CSF were high due to the continuous supply by the pump and, probably due to leakage from tissue binding sites (Fig. 3*C*).

Daily intranasal application of anti-Nogo-A antibodies (1 mg/day) was done for 7 d to compare the distribution and uptake with 7 d of intrathecal application. Antibodies were detectable in all analyzed regions of the CNS, including the cervical, thoracic, and lumbar spinal cord (Fig. 3*D*). Like after intrathecal application, hippocampal and spinal cord concentrations were particularly high probably due to the high density of Nogo-A-expressing pyramidal cells in the hippocampus and high amount of myelin Nogo-A in the spinal cord (Fig. 3 *A* and *D*). When comparing the antibody concentrations after intranasal application with those after intrathecal pump infusion at 7 d, the following observations were made: the anti-Nogo-A antibody concentrations after intranasal application (total amount applied: 7 mg/rat) in the different parts of the CNS were in a similar range like after intrathecal application, except for the cortex (total amount applied: 2.5 to 3mg/rat) (Fig. 3 *A* and *D*). Serum concentrations were lower after intranasal as compared with intrathecal treatment, suggesting that a large part of the nasally applied antibody stayed in the nose or was lost (Fig. 3 *B* and *E*). The amount of antibody detected in the brain and spinal cord after 7 d of daily intranasal application was about 0.15% of the total 7 mg of applied antibody, (Fig. 3*F*).

Application of anti-Nogo-A antibodies in animal models of CNS injury was often done over a period of 14 d (28, 58, 59). We, therefore, evaluated the feasibility of prolonged and repeated intranasal application of anti-Nogo-A or control antibody for 14 d (1 mg/rat/day). A similar pattern of regional antibody distribution and interestingly, also antibody levels were obtained like after 7 d of intranasal application. Anti-Nogo-A antibody tissue levels were higher than those of the control antibody, spinal cord and hippocampus were higher than the other parts of the CNS, except for the olfactory bulbs, which reached the highest values (Fig. 3*G*). Serum concentrations were also similar in the two treatment groups (Fig. 3*H*). 0.016% of the total 14 mg intranasally applied antibodies were

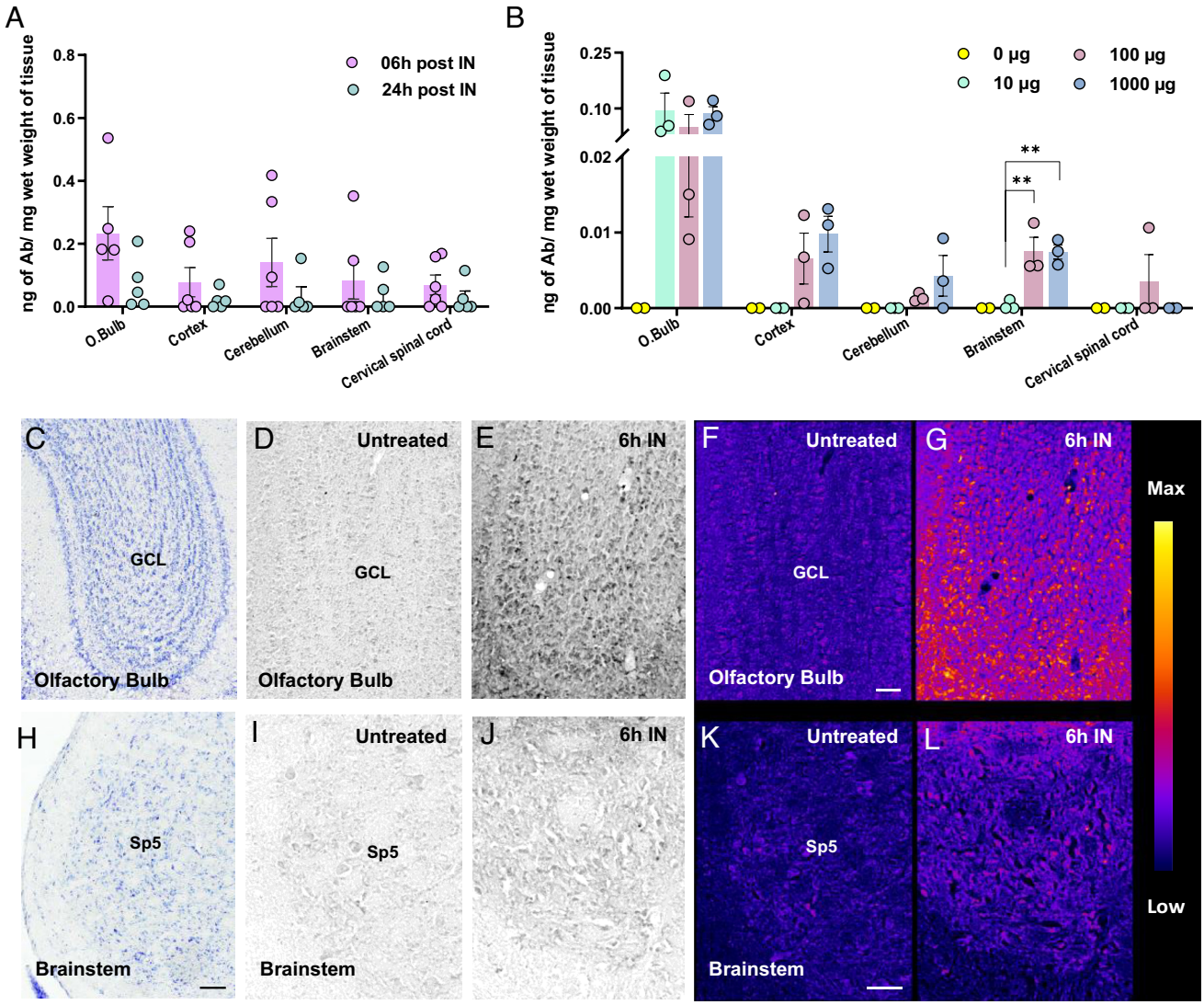

Fig. 1. Quantification and localization of anti-Nogo-A antibody 11C7 by ELISA and immunohistochemistry in the adult mouse CNS 6 h and 24 h after a single intranasal application. (*A*) Concentrations of anti-Nogo-A antibody in different CNS regions 6 h (n=6) and 24 h (n=5) after a single intranasal application (500 µg/nares) as detected by capture ELISA. Statistical evaluation was done using the mixed-effects two-way ANOVA model followed by Bonferroni post hoc correction. (*B*) Regional distribution of anti-Nogo-A antibody 6 h after a single intranasal application at different doses: 0 µg (n=2); 10 µg (n=3); 100 µg (n=3); and 1,000 µg (n=3). One-way ANOVA followed by Bonferroni post hoc correction was used. Data are presented as mean ± *SEM*, asterisks indicate significances: **P* < 0.05, ***P* < 0.01. (*C*–*L*) Detection of biotinylated mouse anti-Nogo-A antibody by histochemistry in adult mouse brain 6 h after a single intranasal application (100 µg; 50 µg/nostril). (*C* and *H*) Nissl stain of the olfactory and brainstem regions. (Scale bar, 100 µm.) (*E*, *G*, *J*, and *L*) Diffuse, as well as a cellular 11C7-biotin signal is found in the granule cell layer of the olfactory bulb (*E* and *G*) and the spinal trigeminal nucleus (*J* and *L*) in the brainstem. (*D*, *F*, *I*, and *K*) Only low background staining is seen in the corresponding brain regions in the untreated mouse. (*F*, *G*, *K*, and *L*). Color-coded staining intensity of HRP–DAB-stained cryostat sections of olfactory and brainstem region. GCL: granule cell layer; Sp5: spinal trigeminal nucleus. (Scale bar, 50 µm.)

present in the CNS tissue at 14 d (Fig. 3*I*). The intranasal application of antibody was well tolerated. Animals were closely monitored for their wellbeing before and after daily intranasal treatment (weight, activity, etc.) and no abnormalities were found.

As shown above, the serum levels of anti-Nogo-A antibodies were about 5 to 50 times higher than the CNS tissue levels. To assess a possible contribution of blood-borne antibodies to the antibodies detected in the CNS, we used immunohistochemical detection of endogenous rat IgG. These antibodies circulate at concentrations around 10 mg/ml; leakage into CNS tissue should therefore be easily detected. While the well-known sites of open BBB were very obvious in these immunohistochemical sections (hypothalamus, lateral ventricle, choroid plexus, cortex), no staining of e.g., cortical, or hippocampal pyramidal cell, cerebellar Purkinje neurons or trapezoid body neurons was observed (*SI Appendix*, Fig. S2).

Intranasal Application of Anti-Nogo-A Antibody Enhanced Functional Recovery of Skilled Forelimb Grasping after Stroke in Adult Rats. To test the efficacy of intranasally applied anti-Nogo-A antibody for functional recovery and structural adaptation after stroke, the antibody 11C7 or a control antibody (isotype control) was used in a thrombotic stroke model in rats. As shown above, daily intranasal delivery for 7 d resulted in CNS tissue concentrations of the antibody approaching the range of 7 d of intrathecally infused antibody. This determined the dose to assess the efficacy of intranasal application. We induced a large unilateral stroke by photothrombosis of the sensory-motor cortex. Rats were then treated daily with an intranasal application of anti-Nogo-A or control antibody for 2 wk. Skilled motor forelimb function was assessed weekly in the single-pellet grasping (SPG) test for 6 wk (Fig. 4*A*). At the end of the behavior assessment, the anterograde axonal tracer biotinylated dextran amine (BDA) was injected into the contralesional, intact fore- and hindlimb motor cortices of the stroke-affected rats to assess reinnervation of the stroke-denervated cervical hemicord and pons by sprouting of contralesional descending corticospinal (CST) fibers (Fig. 4*A*). Lesions induced were large and covered most or all of the sensory-motor cortex. Cortical lesion depth was analyzed using cresyl violet/Nissl-stained brain cross-sections (Fig. 4 *B* and

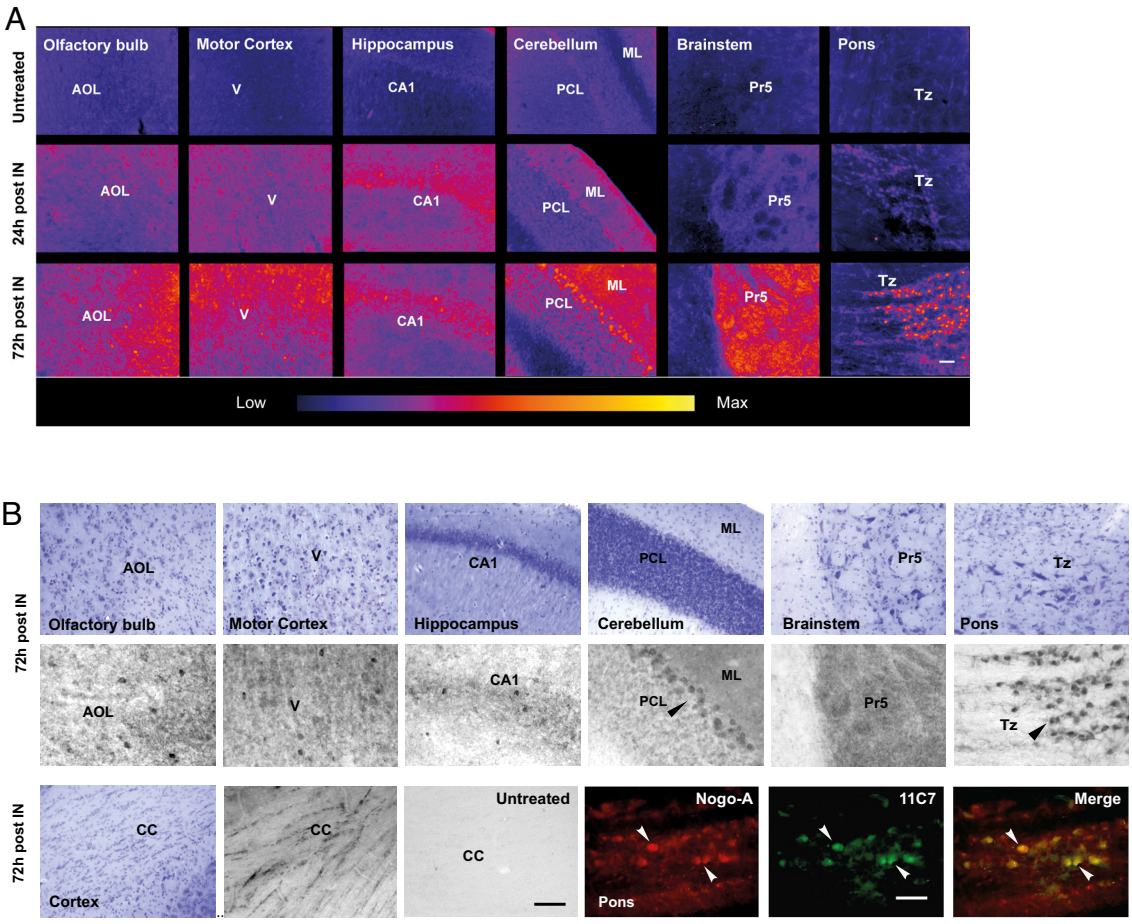

Fig. 2. Localization of mouse anti-Nogo-A antibody 11C7 by immunohistochemistry in the adult rat brain 24 h after a single intranasal application or after three successive daily intranasal applications (72 h). (*A*) Regional distribution of anti-Nogo-A antibody immunoreactivity in the adult rat brain at 24 and 72 h post-intranasal application. Color coding shows the intensity of staining in the olfactory bulb, motor cortex, hippocampus, cerebellum, brainstem, and pons. Sections of untreated rat show low background staining only. (*B*) Mouse antibody 11C7 was detected on/in cells in many brain regions, in particular after repeated intranasal application. Examples shown are from the olfactory bulb, pyramidal cells of lamina V of the motor cortex and CA1 of the hippocampus, Purkinje cells of the cerebellum, and large neurons in the trapezoid nucleus and principal sensory trigeminal nucleus (Pr5). In white matter, e.g., corpus callosum, the typical row-forming oligodendrocytes are also labeled. All these labeled cell types are known to express Nogo-A. Double immunofluorescent labeling of the trapezoid nucleus for endogenous Nogo-A and mouse antibody 11C7 confirmed the colocalization (*Lower Right*). AOL: anterior olfactory nucleus, lateral; (V) Lamina V of motor cortex; CA1: *cornu ammonis* 1 of the hippocampus; ML, molecular layer; PCL, Purkinje cell layer; Pr5: principal sensory trigeminal nucleus; Tz: Nucleus of the trapezoid body; CC: corpus callosum. – Red channel: Nogo-A; Green channel: Mouse IgG (11C7 detection). (Scale bars, 100 μm.)

C). The lesion destroyed all cortical layers down to layer V (>70% of cortical thickness) in all animals. No significant differences were observed between the two experimental groups (Fig. 4*C*), ($P > 0.05$, unpaired two-tailed Student's *t* test).

To assess the efficacy of intranasal application of anti-Nogo-A for the recovery of fine motor skills after a stroke, animals were tested in the SPG task, a well-established test for corticospinal tract-dependent forelimb function (62). On day 2 postlesion, all animals that received a stroke showed a strong (75 to 90%) deficit in the success of SPG compared with baseline. This reflects the ablation of the ipsilesional sensorimotor cortex and CST. The forelimb function of the animals intranasally treated with anti-Nogo-A antibody gradually improved over the course of 6 wk reaching a final mean success rate of 69 ± 6% at day 42 postlesion (Fig. 4*D*). In contrast, the success rate of the animals treated with the control antibody plateaued around day 21 at a low level of performance (25 ± 3%) and showed no further improvement until day 42 (34 ± 6%). The recovery of forelimb control as assessed in the SPG task was therefore significantly higher in the anti-Nogo-A animals, out-performing the control antibody-treated animals at every time point from 14 d postlesion onward (Fig. 4*D*), ($P < 0.01$, two-way ANOVA repeated measure followed by Bonferroni *post hoc)*. There was no correlation between the stroke lesion depth and the final success rate in the SPG task at day 42 poststroke (Fig. 4*E*) ($P > 0.05$, $r = 0.13$, Spearman correlation).

Anterograde Tracing of Contralesional Corticospinal Tract Revealed Increased Sprouting into the Stroke-Denervated Cervical Hemicord and Pons in Intranasally Anti-Nogo-A-Treated Rats. In rats and mice with large strokes, intrathecal anti-Nogo-A antibodies or genetic deletion of Nogo-A were shown to enhance growth and arborization of the contralesional, spared CST fibers into the stroke-denervated spinal cord gray matter or brainstem (28, 58, 63, 64). Here, we investigated if similar plastic fiber growth of CST fibers could be observed after intranasal application of Nogo-A neutralizing antibodies.

The anterograde axonal tracer BDA was injected into the contralesional (intact hemisphere) sensory–motor cortex in all stroke-lesioned, antibody-treated animals (14-d intranasal application of 11C7 or control antibody) at day 42. Rats were fixed by perfusion 3 wk later. Serial cross-sections of the cervical enlargement at levels C3–C4 were analyzed to quantify the labeled CST fibers in the spinal cord midline and the denervated hemicord gray matter (Fig. 5 *A*–*C*). The number of collaterals leaving the main CST and crossing the midline was counted in the dorsal and ventral commissure (Fig. 5*B*, level M), and the branching of these fibers was evaluated at four defined mediolateral positions within the gray matter (Fig. 5*B*, levels D1 to D4, see *Materials and Methods*). BDA-labeled descending CST projections to the stroke-denervated hemicord were observed, (Fig. 5 *D* and *E*) in line with previous studies (28, 58). Midline-crossing fibers and CST fibers in the stroke-denervated

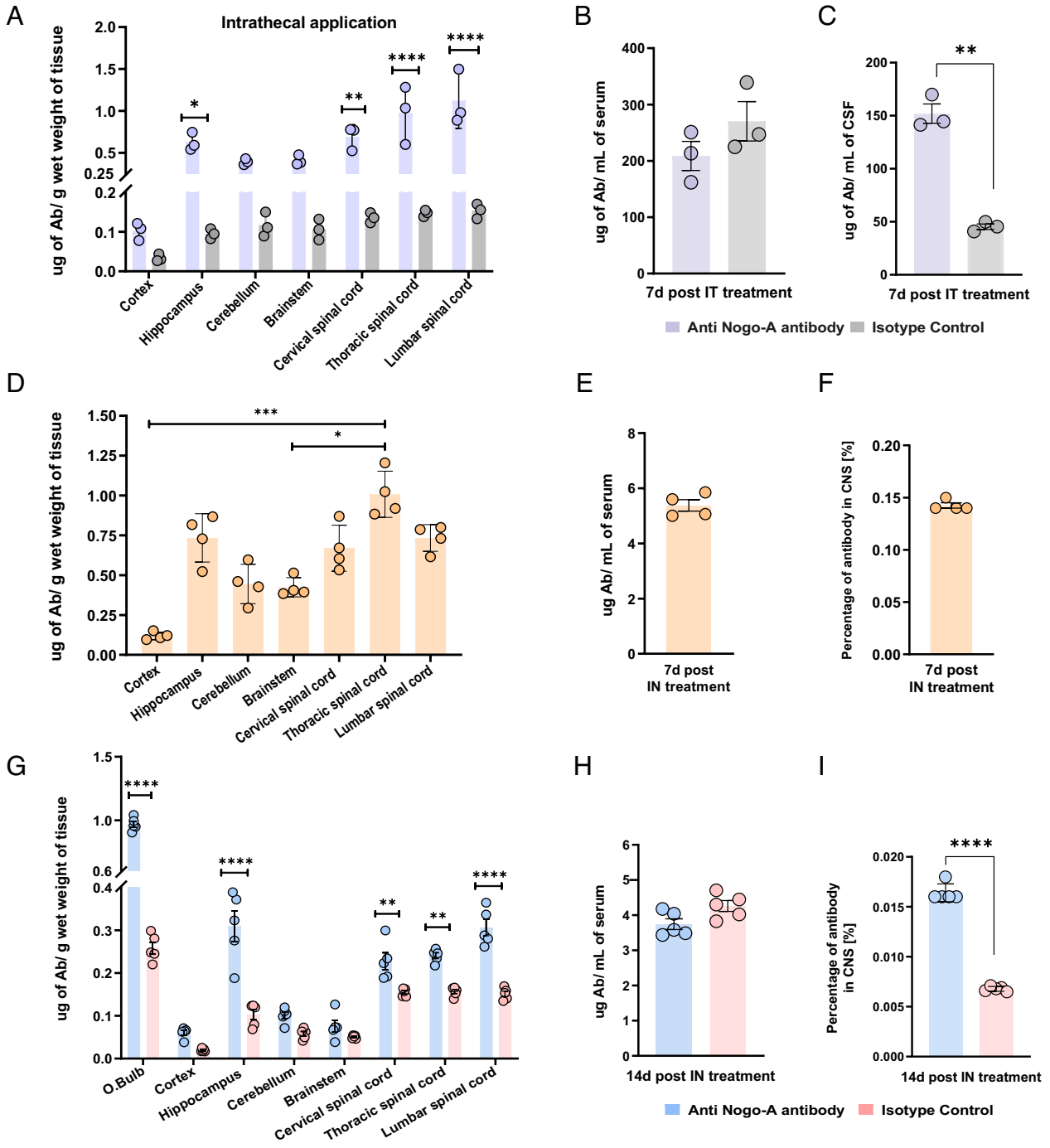

Fig. 3. Regional tissue concentrations of anti-Nogo-A or control antibody following intranasal or intrathecal application. (*A*) CNS tissue concentrations of anti-Nogo-A antibody or isotype control by ELISA in intact rats after 7 d (7d) of intrathecal, lumbar pump infusion (total mount infused: 2.5 to 3 mg). Data are mean values of µg of antibody normalized to gram tissue wet weight ± *SEM*. (*B*) Mean concentrations of anti-Nogo-A and isotype control antibody in the rat serum and (*C*) cerebrospinal fluid (CSF) after 7 d of pump infusion. (*D*) Regional tissue concentrations of anti-Nogo-A antibody in the brain and spinal cord following daily intranasal application (1 mg/day) for 7 d. (*E*) Mean concentrations of anti-Nogo-A in the rat serum. (*F*) Percent of antibodies detected in the CNS (brain and spinal cord), at day 7 of the total 7 mg applied intranasally. (*G*) Regional CNS tissue concentrations of anti-Nogo-A antibody or isotype control in intact rats after 14 d of intranasal application (1 mg antibody/day). (*H*) Mean concentrations of anti-Nogo-A and isotype control in the rat serum ± *SEM*. (*I*) Percent of antibody detected in the CNS at day 14 of the total 14 mg applied via nasal route. Statistical evaluation was done using ANOVA measures followed by Šídák's multiple comparisons test and Student's *t*-test; for the nonparametric test: the Kruskal–Wallis test followed by Dun's correction was used; n=3 to 5; asterisks indicate significances: **P* < 0.05, ***P* < 0.01, ****P* < 0.001, *****P* < 0.0001.

gray matter of segments C3 and C4 were significantly more numerous in the rats treated intranasally with anti-Nogo-A antibody as compared with intranasal control antibody (Fig. 5 *D* and *E*). These results suggest that intranasal application of the growth-enhancing anti-Nogo-A antibody enhanced the formation of new projections arising from the contralesional, intact CST to the gray matter of the stroke-denervated hemicord.

We correlated the behavioral performance in the skilled reaching test after the stroke with the numbers of CST fibers projecting across the midline to the stroke-denervated spinal hemicord at levels C3–C4. There was a positive correlation between the numbers of BDA-labeled CST fibers in the stroke-denervated gray matter and the success rate for skilled reaching at day 42 in the individual animals (*SI Appendix*, Fig. S3). The correlation was

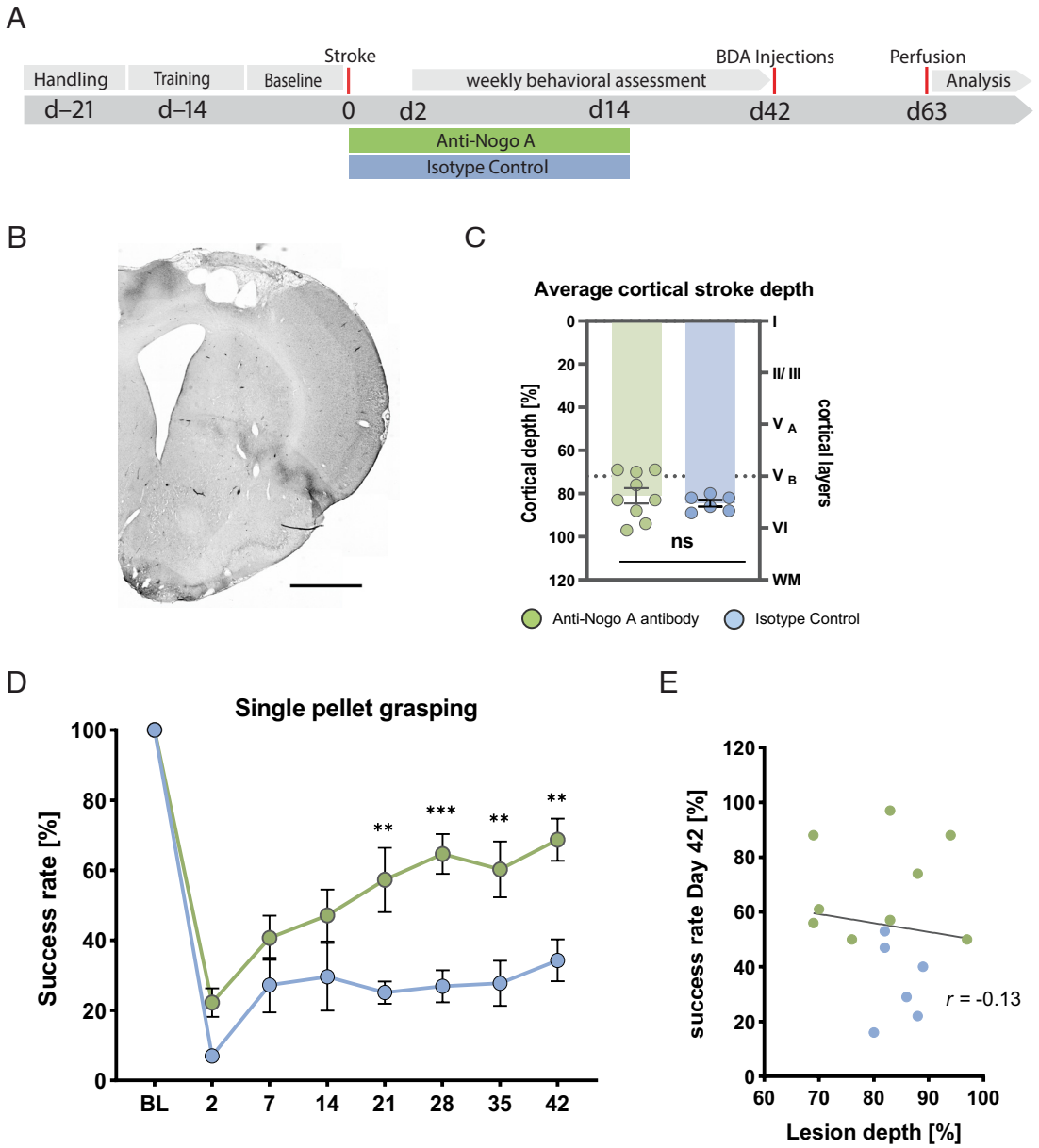

Fig. 4. Intranasal application of anti-Nogo-A antibody enhanced functional recovery. (*A*) Experimental timeline (d: days), adult rats received large unilateral cortical strokes followed by 14 d of intranasal application of either anti-Nogo-A antibody or control antibody. Weekly behavioral assessment was carried out starting from day 2 to day 42 poststroke. At the end of the behavioral assessment anterograde tracing of the CST fibers was carried out for neuroanatomical analysis in the cervical spinal cord. (*B*) Representative coronal section of a brain depicting cellular damage throughout the layers of the sensorimotor cortex 63 d poststroke. (Scale bar, 1.5 mm.) (*C*) Quantification of cortical stroke depth. Dotted line represents the position of ipsilesional corticospinal motor neurons (cortical layer V). (*D*) Success rate in the SPG task at baseline (BL; intact, trained) and after a unilateral photothrombotic stroke to the sensorimotor cortex of the preferred paw from day 2 to Day 42 postlesion of anti-Nogo-A antibody (green, n = 9) or control antibody (blue, n = 6)-treated animals. Data are presented as mean ± *SEM.* Statistical evaluation was carried out with two-way ANOVA repeated measure followed by Bonferroni *post hoc,* asterisks indicate significances: $^{**}P < 0.01$ and $^{***}P < 0.001$. (*E*) No correlation was found between the lesion depth and the success rate on the SPG task at day 42 poststroke ($P > 0.05$, $r = 0.13$, Spearman correlation).

highest for the midline and the D2 region in both segments (*SI Appendix*, Fig. S3 *A*, *C*, *D*, and *F*). Our results suggest that the plastic rewiring and side-switch of intact CST fibers which are enhanced by the intranasally applied anti-Nogo-A antibodies may contribute to the higher recovery of skilled forelimb reaching observed under these conditions.

Inactivation of Nogo-A in animals with large strokes was shown to lead to enhanced plasticity and midline crossing of corticofugal fibers also in the brainstem, e.g. in the pons (63). We analyzed the BDA-labeled corticofugal fibers originating in the contralesional, intact forelimb motor cortex projecting to basilar pontine nuclei in the rats treated intranasally with anti-Nogo-A or the control antibody, respectively. We quantified these fibers in the four typical termination zones of the basilar pons, the central and the medial nucleus, the lower, denser lateral region (lateral 1), and an upper, lighter region (lateral 2). Fiber counts were normalized to the number of BDA-labeled corticofugal fibers in the cerebral peduncle. The terminal fields were dense on the ipsilateral side to the injection, and a few fibers crossing the midline and terminating contralaterally were seen (Fig. 6 *A* and *B*), in line with published results (65, 66, 67). The anti-Nogo-A-treated group showed higher numbers of corticopontine projections to stroke-denervated central and medial basilar pontine nuclei as compared with the control antibody-treated rats (significant for the central, only tendency for the medial nucleus; Fig. 6*C*). The number of intact forelimb cortical projections to the stroke-affected central nucleus

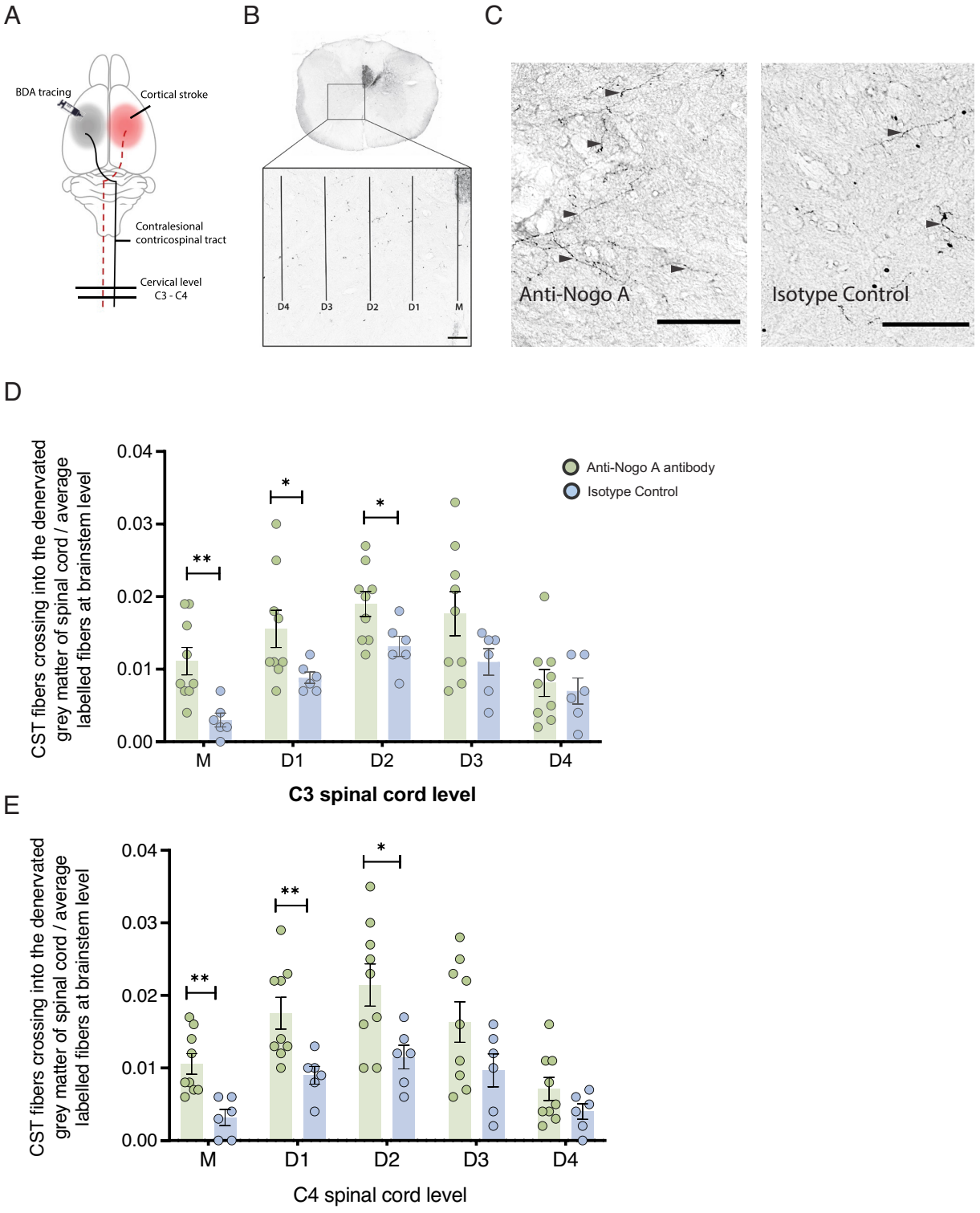

Fig. 5. Intranasal application of anti-Nogo-A for 2-w. enhanced contralesional CST sprouting into the denervated hemicord after stroke. (*A*) Anterograde axonal tracer BDA was injected into the contralesional (intact hemisphere) sensory–motor cortex and the cervical segments C3–C4 were analyzed to quantify CST fibers in the midline and the stroke-denervated hemicord. (*B*) Low magnification micrograph of BDA-labeled corticospinal fibers from intact spinal hemicord (*Right*) reinnervating the stroke-denervated hemicord (*Left*; *Inset*) at spinal cord level C3. CST fibers were counted as intersections with vertical lines placed at the midline (M) and given distances in the gray matter (D1 to D4). (Scale bar, 100 μm.) (*C*) Representative micrographs showing corticospinal fibers (arrowheads) from the contralesional cortex in the denervated cervical spinal cord (C3) in anti-Nogo-A and control antibody-treated animals. (Scale bar, 100 μm.) (*D* and *E*) Number of CST collaterals projecting over the midline (M) and innervating the denervated gray matter at D1 to D4 in anti-Nogo-A and control antibody-treated animals at cervical level C3 (D) and C4 (E) normalized to 10% of BDA-positive labeled CST fibers at the brainstem level. Intranasally treated animals with anti-Nogo-A showed significantly more fibers at M, D1, and D2. To account for the variability of BDA labeling in the corticofugal pathway, we determined the number of BDA-positive fibers in the cerebral peduncle at the level of the midbrain. Cervical spinal cord fiber counts were normalized to 10% of the labeled corticofugal fibers. Data are presented as mean ± *SEM*, (green dots: individual animals treated with anti-Nogo-A and blue dots: control antibody); statistical evaluation was carried out with Student's *t*-test (two-tailed, unpaired), asterisks indicate significances: $*P < 0.05$ and $**P < 0.01$.

correlated positively with the success rate of skilled forelimb grasping at 42 d poststroke (Fig. 6*D*; ***$P = 0.0006$, $r = 0.86$, Pearson correlation). These results suggest that plastic changes in the brainstem, which are enhanced by intranasal application of anti-Nogo-A antibody, contribute to the observed functional recovery.

Discussion

Therapeutic antibodies targeting CNS antigens are of high current interest for several neurological diseases. Easy and noninvasive routes of application would be highly desirable. Our study revealed three major findings. First, intranasally applied full-size IgG anti-Nogo-A antibodies reached the brain and spinal cord in intact adult rats and mice after single as well as multiple applications. Second, daily intranasal delivery for 7 d resulted in CNS tissue concentrations of the antibodies approaching the range of 7 d of intrathecally infused antibodies. The procedure was well tolerated by the animals. Third, intranasal application of anti-Nogo-A antibodies over 2 wk enhanced compensatory sprouting and significant functional recovery in rats following large cortical stroke.

A rapid transfer of anti-Nogo-A antibodies from the nose to different CNS regions in mice and rats was observed following a single intranasal application. As determined by a highly sensitive capture ELISA, antibody titers tended to be higher at 6 h after intranasal administration than at 24 h, particularly in the olfactory bulb, indicating rapid clearance or uptake and intracellular degradation. Antibody levels increased in a dose-dependent manner, except in the olfactory bulbs where the uptake for the specific antibody used seemed to saturate at an intranasal dose of 10 µg, suggesting that the uptake and transport of the antibodies are time and dose-dependent. Biotinylated mouse anti-Nogo-A antibodies were detected by histochemistry in the olfactory bulb and the trigeminal region of the brainstem in adult mice 6 h after intranasal application, suggesting that these regions are the ports of entry of the antibodies into the CNS. Vectorial antibody movement mainly in the peri- and endoneurium spaces along the olfactory and trigeminal nerves have been shown (35) (49). In the current study, 24 h after a single intranasal application, mouse antibodies were detectable in most CNS regions of adult rats including the spinal cord. The signals were increased after daily applications over 3 d. The histological findings were confirmed by biochemical determinations by ELISA after daily applications over 7 or 14 d. Antibody levels were higher for the anti-Nogo-A antibodies than for the unspecific control IgGs, in line with the binding of the anti-Nogo-A antibodies to their target protein on neurons and oligodendrocyte membranes.

Anti-Nogo-A antibodies also reached the deep regions of the CNS and the spinal cord, suggesting a rapid distribution and tissue penetration. Perivascular spaces were suggested as sites of radial tissue penetration (49), a concept that is well in line with the present findings. Higher concentrations of anti-Nogo-A antibodies were overserved in the hippocampus and the spinal cord. In the adult hippocampus, neuronal Nogo-A and its receptors NgR1 and S1PR2 negatively modulate structural and synaptic plasticity (68–70). Neutralization or ablation of Nogo-A or NgR1 promoted axonal growth, dendritic branching, spine turnover rate, and density (71, 72). Anti-Nogo-A antibody treatment increased Long-term potentiation (LTP) in the hippocampus, as well as in the motor cortex along with improved learning of skilled movements in rats (73). Intranasal anti-Nogo-A antibodies might, therefore, also allow the development of therapies targeting cognitive impairments. Hippocampal function is affected in diseases such as early Alzheimer's disease. Enhancement of structural plasticity in all CNS regions could be of therapeutic value e.g., for traumatic brain injury and stroke.

Especially at the later time points, intranasally applied anti-Nogo-A antibodies were often found to label cell bodies of neurons, e.g., cortical or hippocampal pyramidal cells, cerebellar Purkinje cells, or large neurons in the brainstem and spinal cord, as well as of oligodendrocytes. All these cell types are known to express

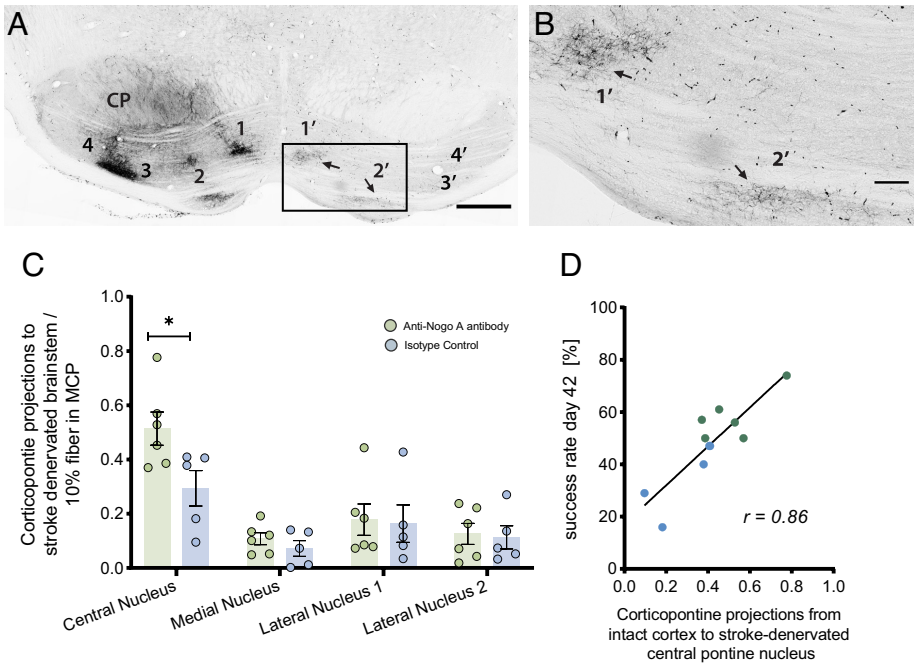

Fig. 6. Anterogradely labeled projection from the intact, contralesional forelimb motor cortex to the pons. (*A*) Micrograph showing cross-section at the mid-pontine level of anti-Nogo-A antibody-treated animal 63 d poststroke. In addition to the strongly labeled intact side, fibers crossing the midline and innervating the central and medial pontine nuclei of the stroke-denervated side (arrows) can be seen. (CP): cerebral peduncle; (1, 1′): Central pontine nucleus; (2, 2′): Medial pontine nucleus; (3, 3′): Lateral pontine nucleus -1; (4, 4′): Lateral pontine nucleus -2. (1-4: intact side; 1′-4′: stroke-denervated side). (Scale bar, 500 µm.) (*B*) Magnification of the boxed region depicted in (*A*), showing crossed fibers terminating and arborizing in the central and medial basilar pontine nuclei (arrows). (Scale bar, 100 µm.) (*C*) Qualification of projections from the intact, contralesional forelimb cortex to the stroke-denervated central, medial, and lateral basilar pontine nuclei, normalized to the number of fibers counted in 10% of the area of the midbrain cerebral peduncle. Level of significance: *$P = 0.01$, two-way ANOVA multiple comparisons followed by Šídák's correction. (*D*) Significant positive correlation of ipsilesional corticopontine projections to the central nucleus to the success rate of skilled forelimb grasping at 42 d poststroke (***$P = 0.0006$, $r = 0.86$, Pearson correlation).

Nogo-A (60, 74). The observed labeling reflects cell surface binding as well as subsequent accumulation by internalization (60, 74, 75). This was confirmed in the current study by showing the co-labeling of the large trapezoid body neurons for antibody 11C7 as well as endogenous Nogo-A protein. The relatively high levels of Nogo-A antibodies found in the spinal cord point to a very efficient transport of the intranasally applied antibody to all parts of the CNS, probably via the CSF circulation. The high amounts of tissue-bound antibodies could be due to the high proportion of oligodendrocytes and white matter in this compartment. To control for a possible systemic way of antibody entry into the CNS, we assessed the relevant CNS regions for the presence of endogenous rat IgG. Rat IgG is present in the blood at high concentrations (around 10 mg/mL); using the same immunohistochemical procedures, reaction, and exposure times as for the visualization of the intranasally applied antibody 11C7, we were unable to show labeled areas or cell bodies. The finding confirms the tightness of the BBB for antibodies and excludes that a significant proportion of the signals observed after intranasal antibody application originates from blood-borne material.

The direct comparison of the antibody amounts reaching the CNS after the intranasal or intrathecal application (for 2 wk) showed similar ranges of tissue-bound anti-Nogo-A antibodies. This led to the crucial question if intranasal application could lead to efficacious concentrations in the CNS and can enhance structural plasticity and functional recovery after CNS injury, as shown earlier with intrathecal antibody application. The present results show that in rats with a large photothrombotic stroke of the sensorimotor forelimb cortex, the daily intranasal application of anti-Nogo-A antibodies for 2 wk induced significant functional recovery of food pellet reaching, a well-established read-out for skilled, cortically controlled forelimb movements. Recovery of forelimb precision movements was shown in earlier studies to be linked with plastic fiber growth into the stroke-denervated spinal cord and brainstem (28, 76, 77, 78). This anatomical plasticity was enhanced by the suppression of Nogo-A (58, 63, 79). Accordingly, pharmacogenetic silencing of the midline crossing CST fibers eliminated functional recovery (28). We observed similar enhanced compensatory sprouting of corticospinal fibers in the cervical spinal cord and of corticobulbar fibers in the pons after intranasal anti-Nogo-A application. These plastic changes correlated with functional recovery of skilled forelimb grasping in the individual rats. The central basilar pontine nucleus, where the most prominent sprouting was observed, is known to be a major termination area for forelimb projections to the pons (65, 66, 67, 74). In addition, these projections highly correlated with skilled forelimb grasping in the stroked rats. In the current study, intranasally applied anti-Nogo-A antibodies reached the motor cortex, brainstem, and cervical spinal cord, thus allowing plastic changes, sprouting, and rewiring to occur at the cortical, brainstem, and spinal levels. These results show that repeated, daily intranasal application of anti-Nogo-A antibodies for 2 wk results in CNS antibody concentrations, which enhance structural plasticity and functional recovery in the corticofugal system similar to earlier results with intrathecal antibody infusion.

To date, the intranasal application of CNS targeting drugs in humans has been limited mostly to small molecules in clinical trials (51). Despite the efforts made in the past in understanding the transport mechanisms, CSF distribution as well as uptake within the brain parenchyma of intranasally applied molecules, the field lacks efficacy studies for defined macromolecular CNS-targeting therapeutics. With the development of target-specific therapies for neurological disorders, particularly monoclonal antibodies for Alzheimer's disease, Parkinson's disease, Multiple sclerosis, or CNS trauma, further research is much needed to validate the therapeutic effects of noninvasive application routes, such as the intranasal application. Preclinical studies with single or multiple doses examining pharmacokinetics, mucosal toxicity, uptake and transport mechanisms, CNS distribution, and therapeutic efficacy in different animal models are needed. Permeability enhancers have also been used in several studies (48, 49, 80). The use of nasal enhancers/emulsifiers under conditions of the specific pathologies to be treated needs to be explored; effective compounds might be irritant or associated with long-term damage to mucosal or sensory olfactory tissues. Furthermore, the pros and cons of mucoadhesive polymers and drug carriers in nasal formulations together with long-term tolerability need to be addressed. Nasal formulations might have an impact on nasal *pH*, local immune surveillance, mucociliary clearance, or secretions of the olfactory mucosa.

A key question is also how comparable or relevant results obtained in rodent studies are for the primate and human situation. The olfactory and respiratory mucosal system in humans is smaller than in rodents compared with head or body size. Still, the human olfactory epithelium (10 cm^2) and the respiratory epithelium (>100 cm^2) (81) represent appreciable surfaces for binding and uptake of small and large bioactive molecules. Indeed, studies have shown the transfer of intranasally applied macromolecules from the nasal epithelium to the olfactory bulb and CNS in nonhuman primates (35, 82). In human studies, direct CSF measurements have shown a rapid appearance of the peptides Melanocyte-stimulating hormone, vasopressin, and insulin after intranasal application; and in pilot clinical studies intranasal insulin was shown to reduce memory loss after long-term application in Alzheimer's patients (41, 83), as well as a reduction in nicotine craving after a single application (84). More studies are needed, but the available evidence clearly argues in favor of the high relevance of rodents as a model for primates including humans when studying nose-to-brain transfer mechanisms and proof-of-concept experiments.

The present results show that therapeutically relevant amounts of intranasally applied therapeutic antibodies can reach all parts of the CNS including the spinal cord in sufficient amounts to enhance compensatory fiber sprouting and functional recovery after large strokes in rats similar to intrathecally applied antibodies. These findings demonstrate the usefulness of the noninvasive intranasal route for bringing therapeutic antibodies to their CNS targets in neurological conditions. They confirm the high interest of this route for delivering biologics to the CNS and will hopefully lead to more translational research for testing, optimizing, and validating such findings in different preclinical models and to their successful translation to clinical studies.

Materials and Methods

Experimental Set-Up. A total of n=60 adult female Long–Evans rats (200 to 250 g, 12 to 16 wk old, Janvier, France) and 30 adult C57/BL6J female mice: n=14, 22 to 26 g; male mice: n=16, 29 to 35 g, 25 wk old, Charles River, Germany), were used in this study. This study was in accordance with the ARRIVE guidelines for reporting animal studies. Additionally, all experimental procedures were approved by the local veterinary office, Canton of Zurich, Switzerland and, in accordance with the Stroke Therapy Academic Industry Roundtable criteria (1999) for preclinical stroke investigations.

The primary objective of this study was to assess a noninvasive route to bring antibodies into the CNS. A highly specific, function-blocking monoclonal antibody, 11C7, directed against the Nogo-A-specific region of rat Nogo-A (54) was used. Adult anesthetized rats received single as well as multiple intranasal applications of anti-Nogo-A antibody 11C7. Antibody uptake was analyzed by immunohistochemistry and by quantitative measurement of antibodies in the blood and CNS tissue. Application of anti-Nogo-A antibody in animal models of CNS injury was often done over a period of 14 d (28, 55, 58, 59). We, therefore, evaluated the feasibility of prolonged and repeated intranasal application of anti-Nogo-A or control antibody for 14 d.

The beneficial effects of a temporal suppression of Nogo-A signaling in different CNS lesion paradigms and species including nonhuman primates have been shown by several laboratories over the last >20 y. Previous work on the effect of anti-Nogo A antibodies in sham-operated/nonstroked animals has been shown in the past together with training/rehabilitation therapies. The objective of the intranasal stroke study was to examine the effect of intranasally applied anti-Nogo-A antibody treatment after a stroke for the restoration of skilled forelimb function.

All animals received training in SPG followed by a photothrombotic stroke and the intranasal application of anti-Nogo-A antibody or IgG control antibody as described below. Animals were then randomized into two different treatment groups. This experimental setup was repeated in two independent studies with n = 15 rats per cohort for behavioral and morphological analysis, the data shown here were pooled from two cohorts. Animals were number-coded, and investigators were blinded to the treatment groups throughout the experiment until the completion of data analysis.

Defining Exclusion Criteria. All animals that showed a 60 to 80% deficit in success rate in pellet grasping at day 2 postlesion were included. Animals that achieved superior performance on day 2 or had a stroke depth of <65% of the cortical thickness (see below) were excluded from further analysis. Furthermore, we observed variability in the BDA tracing of CST used for the analysis of neuroanatomical reorganization of CST-dependent forelimb function. A few animals with very low numbers of labeled CST fibers were also excluded. A total of 14 of the original 30 animals lesioned were excluded. Two mice out of in total 30 mice with absolute values below the detection limit in the olfactory bulb region were excluded from the ELISA study analysis.

Intranasal Administration of Antibody. The intranasal application was carried out in anesthetized mice and rats. Animals were briefly anesthetized with 5% isoflurane followed by injection anesthesia using intraperitoneal *(i.p.)* injection of medetomidine (0.5 mg/kg body weight) and ketamine (100 mg/kg body weight) for mice, and intramuscular *(i.m.)* injection of medetomidine (150 μg/kg body weight) for rats to achieve a light sedative effect. Body temperature was maintained at 37 °C on a heating pad. Animals were placed in a supine position, which allowed for easy breathing as well as easy access to the nostrils of animals. For the mouse study, a total of 24 μL (0.42 mg/mL, 4.16 mg/mL, and 4.167 mg/mL biotinylated anti-Nogo-A antibody 11C7 or Phosphate-buffered saline) was applied in three 4 μL drops per nare, alternating every 5 min using sterile gel loading pipette tips. In rats, 100 μL antibody (10 mg/mL anti-Nogo-A antibody 11C7 or FG12/B5 mouse IgG1 isotype control antibody) was applied to alternating nares in 10 μL drops every 2 min for 20 min using sterile gel loading pipette tips.

The antidote atipamezole was administered subcutaneously (*s.c.)* and the animals were taken to the dedicated wake-up cage equipped with a heating pad set to 38° C. To counteract pica behavior, all bedding material was removed, and the animals only had access to food pellets placed on the floor and the water. After full recovery from the sedation, the rats were taken to their home cages.

Intrathecal application of antibodies was performed as previously described (28), A total amount of 3 mg antibody/rat was applied over 7 d. A short description can be found in the Supplement.

Perfusion and Tissue Processing. Mice and rats were terminally anesthetized using inhalation of 5% isoflurane and were subsequently injected with a deadly overdose of Pentobarbital, *i.p.* (250 μL for mice, 1 mL for rats, (Esconarkon 300 mg per 1 mL, Streuli Pharma AG). They were perfused transcardially with 30- or 150-mL Ringer solution (containing, 5% Heparin (B. Braun, 25,000 I.E.,/5ml), followed by 100 or 300 mL of a 4% phosphate-buffered paraformaldehyde (PFA) solution, *pH* 7.4. Brains and spinal cords were dissected, kept in 4% PFA for post-fixation for 24 h, and transferred to 30% sucrose (Sigma) in phosphate buffer at 4 °C cryoprotection until further processing.

For quantitative analysis of anti-Nogo-A antibody in CNS tissue by ELISA, mice and rats were transcardially perfused with 30- or 150-mL Ringer solution containing, 5% Heparin (B. Braun, 25,000 I.E.,/5mL). The brain and spinal cord were quickly removed, placed on ice, and divided into anatomical regions. The samples were snap-frozen in liquid nitrogen and stored at −80 °C until further processing.

Histological Analysis of Anti-Nogo A Antibody Uptake in Mouse Brain. For the detection of the biotinylated monoclonal anti-Nogo A antibody in the brain 6 h after intranasal application, mice were perfused and fixed as described above, and 20-μm cryostat sections of the brains of both treated and untreated animals were stained by on-slide processing using the nickel-imidazole-enhanced DAB (3,3′- diaminobenzidine) protocol. Briefly, sections were rinsed in TBS-T (0.05M tris-buffered saline + 0.3% Triton-X, *pH* 8.0). Following unmasking steps using 50 mM NH_4Cl dissolved in 0.1M PB and a 50 mM Tris-glycine incubation, the ABC Elite-DAB peroxidase detection system (1:100, Vector Laboratories) was incubated overnight at 4 °C. Subsequently, the tissue was reacted in 0.01% ammonium nickel sulfate (Sigma-Aldrich), 0.007% Imidazole (Sigma-Aldrich), 0.05% DAB (Sigma-Aldrich), and 0.004% H_2O_2 in 50 mM Tris buffer, *pH* 8.0. Slides were dehydrated in a graded alcohol series, cleared in xylene, and coverslipped with Eukitt (Faust) mounting medium. Mosaic images of cross-sections of the mouse brains and spinal cords were obtained (Zeiss, Axio Scan.Z2, brightfield, 20× magnification) for the detection and analysis of the anti-Nogo A antibody signal distribution.

Histological Analysis of Anti-Nogo-A Antibody Uptake in Intact Rat Brain. For the detection of the mouse monoclonal anti-Nogo-A antibody in the brain after intranasal application, rats were perfused and fixed as described above, and 40-μm cryostat sections of the brains of both treated and untreated animals were stained free-floating with a rat adsorbed anti-mouse IgG antibody coupled to biotin (1:300; Jackson ImmunoResearch), followed by the ABC Elite-DAB peroxidase detection system (Vector Laboratories). Tiff Images were captured using a Zeiss Axioscope microscope (20× Objective) coupled to an OPTRONICS camera at constant exposure time (Neurolucida). Comparative regional antibody distributions in brain regions after intranasal delivery of anti-Nogo-A antibody were analyzed in peroxidase-DAB-stained sections. Signal intensities were measured by ImageJ and color-coded. Mouse IgG immunoreactivity in all brain regions was detected in animals treated intranasally with anti-Nogo-A. The parallel-processed control animal showed no signal except a few endogenous peroxidase-positive erythrocytes.

Analysis of Anti-Nogo A Antibody Uptake in Nogo-A-Positive Neurons. For double immunofluorescence, staining sections were incubated overnight with a primary anti-serum against Nogo-A (Laura Rabbit Serum, 1:1,000) (54) in Tris 50 mM *pH* 7.4 containing 5% goat serum and 0.05% Triton X100, followed by affinity-purified goat anti-mouse IgG antibodies (Jackson Laboratories) coupled to Alexa 488 (1:500) and goat anti-rabbit IgG antibodies coupled to Cy3 (1:300) for 1 h at room temperature. Sections were washed and coverslipped with Mowiol. Images were captured using a Zeiss microscope (Plan NEOFLUAR 40× objective).

Detection of Infused anti-Nogo-A Antibodies in Serum, CSF, and CNS Tissue by ELISA. Detection of antibodies in CNS was carried out as previously described (59). Briefly, the tissue was homogenized in a weight-to-volume ratio of 1:3 in modified lysis buffer containing 200 mM sodium chloride, 20 mM Tris-HCl, *pH* 8.0, 1% NP-40, 1 mM EDTA, and protease inhibitors (Roche, Basel, Switzerland). All homogenizations were prepared on ice. The homogenate was centrifuged in a tabletop-refrigerated centrifuge at the maximum speed for 1 h (16,000 rpm at 4 °C) to pellet the cell and tissue debris (maximally 15 to 25% of the total homogenate). The protein concentration in the supernatant (between 75% and 85% of the total homogenate) was measured with the RC-DC Protein Assay Kit (Bio-Rad).

The concentration of anti-Nogo-A antibodies in serum, CSF, and CNS tissue was measured with a sandwich ELISA. Detection of 11C7 in mice was carried out using the highly sensitive sandwich ELISA with 3× amplification. Briefly, 3 μg/mL rat Nogo-A delta-20 fragment was coated on a high-binding half-area plate (Corning) and blocked using 5% w/v skimmed milk powder in TBS-T buffer (Tris-buffered saline, 0.1% Tween 20), followed by incubation of CNS samples and a serial dilution of the 11C7 anti-Nogo-A antibody (from 3 ng/mL to 0.0046 ng/mL) as an internal standard. Capture and detection of anti-Nogo-A antibodies were carried out using three polyclonal amplification antibodies, rabbit anti-mouse (1:5,000, Invitrogen), goat anti-rabbit (1:5000, Invitrogen), and horseradish peroxidase (HRP)-conjugated donkey anti-goat antibody (1:1,000, Invitrogen). In the rat study, plates were coated with rabbit anti-mouse IgG (1:2,000, Invitrogen) as the primary antibody and blocked using 5% w/v skimmed milk powder in TBS-T buffer (Tris-buffered saline, 0.1% Tween 20) followed by incubation of samples. To detect the anti-Nogo-A antibodies in the samples, a HRP-conjugated goat anti-mouse IgG (1:2,000, Invitrogen) secondary antibody was used. Between each incubation step, the plates were washed thoroughly with TBS-T buffer. The activity of HRP was determined by a Pierce™ 3,3′,5,5′ tetramethylbenzidine substrate (Thermo Scientific), and the optical density of the HRP reaction was determined at 450 nm using a Tecan Spark® plate reader. The concentrations of anti-Nogo-A antibodies in serum, CSF, and CNS tissue were then plotted against a standard curve of anti-Nogo-A antibodies.

Photothrombotic Stroke. Animals were anesthetized with 3% isoflurane, followed by an *i.m.* injection of a triple-shot consisting of medetomidine (150 μg/kg body weight), midazolam (2 mg/kg body weight), and fentanyl (5 μg/kg body weight). Body temperature was maintained at 37 °C on a heating pad. A photothrombotic stroke to unilaterally lesion the sensorimotor cortex corresponding to the preferred paw (see "behavior training" section) was induced as previously described (58). A short description of this procedure can be found in the Supplement.

Behavior Training and Analysis.

SPG task. All animals were trained in the SPG task to assess fine motor control of the forelimb. Animals were placed in a Plexiglas box (34 × 14 cm) with two

openings on opposite ends and had to grasp pellets (45-mg dustless precision pellets, TSE Systems Intl. Group) one by one alternating between the two cage windows. During testing sessions, animals were given 20 pellets within a maximum time of 20 min. Grasping performance was scored as previously described (85). Briefly, a trial, defined as the animal put its paw through the grasping window to grasp a new pellet presented to the preferred side was scored as 1 (successful grasp) if the animal retrieved the pellet and brought it directly to its mouth. A score of 1 was also given if the animal required several attempts to grasp the pellet, without retracting the paw through the window and into the box, which was defined as the end of the attempt. A score of 0.5 was given if the animal successfully grasped the pellet but dropped the pellet inside the box. If the animal knocked the pellet off the shelf, the trial was scored as 0. All testing sessions were filmed (Panasonic HDC-SD800 High-Definition Camcorder, 1920 × 1080, 60 fps). The success rate was calculated as the percentage of retrieved pellets of the number of all trials, which was normalized to baseline. Animals were trained for 3 to 4 wk for baseline recordings before the stroke. During this time, their handedness was recorded. Stroke was induced on the contralateral motor cortex aiming to mainly impair the function of the dominant hand. Handedness was determined ahead of training. Rats were trained until they achieved a success rate of about 80%. Rats were then randomized into two groups (anti-Nogo-A and control IgG antibody group). The blinding of experimenters was strictly kept up throughout the experiment.

Analysis of sprouting patterns in the cervical spinal cord and brainstem. Growth and sprouting of BDA-positive CST fibers to stroke-denervated hemicord in response to stroke and intranasal anti-Nogo-A treatment were evaluated in three adjacent cross-sections at the caudal cervical enlargement C3 to C6. Midline-crossing fibers were manually counted in the dorsal and ventral commissure at the central canal (see Fig. 5*B* level M) and the branching of these fibers was evaluated at four defined regions within the gray matter (28), (see Fig. 5*B* levels D1 to D4). Six vertical lines (M, D1 to D4, and L) were superimposed on each spinal cord section using ROI manager in FIJI (ImageJ) as reference points for crossing axons. The first vertical line M was drawn through the central canal; L was drawn parallel to M and at the lateral rim of the gray matter. D1 to D4 were drawn parallel to M, at one-fifth, two-fifths, etc. of the distance between M and L (Fig. 5*B*). CST fibers in the gray matter have an irregular course, passing in and out of the plane of the section. To prevent multiple counting of single collaterals, only fibers that crossed M, D1, D2 D3, and D4 were counted on each section.

For the analysis of corticopontine projections to stroke-affected basilar pontine nuclei, three consecutive sections with clearly visible basilar pontine nuclei on the ipsilateral side to the BDA injection were chosen. Using ROI Manager in FIJI (ImageJ), four defined nuclei were selected on the ipsilateral to the BDA injection side and mirrored to the contralateral side of the section to ensure the proper location of the nuclei for the manual count of fibers (Fig. 6*A*). The central and medial nuclei were analyzed as one region of interest, the lateral was split in 2 – a lower, denser (lateral 1), and upper lighter (lateral 2) region (Fig. 6*A*). To correct for variations in BDA labeling, we normalized the data (pons and cervical spinal cord) to the number of BDA-labeled fibers counted in 10% of the area of the whole cerebral peduncle. The cerebral peduncle on the level of the midbrain had a cross-sectional area of about 300,000 μm^2. On the ipsilateral to the BDA injection side of the brain, in this area of the cerebral peduncle, labeled fibers in five regions of 6,000 μm^2 each were counted, which amount to 10% of the cerebral peduncle BDA-labeled corticofugal fibers. This value was later used as a normalization factor in the analysis of the midline crossing fibers.

Photothrombotic stroke, intrathecal administration of the antibodies, neuroanatomical tracing, and histology of labeled corticospinal tract were performed according to published protocols. More details regarding these procedures can be found in *SI Appendix*.

Statistical Analysis. Statistical analysis was performed with GraphPad Prism Software. For comparing the behavioral recovery of treatment groups, a two-way ANOVA followed by Bonferroni post hoc correction was used for pair-wise comparisons whenever a main effect or interaction achieved statistical significance. Whenever two treatments or doses were compared at a single one-time point or defined region of interest, one-way ANOVA followed by Bonferroni post hoc correction or Student's *t*-test (two-tailed, unpaired) or Welch's unpaired *t* test was used. For comparing the quantitative measurement of antibodies in a CNS compartment between two treatment groups, two-way ANOVA followed by Sidak's multiple comparisons correction was used; for the nonparametric test: the Kruskal–Wallis test followed by Dun's correction was used; and Spearman or Pearson correlations between the behavioral recovery and the lesion volume and the anterogradely labeled fibers. Data are presented as mean ± *SEM*, single data points represent single animals, and asterisks indicate significances: $*P \leq 0.05$, $**P \leq 0.01$, $***P \leq 0.001$, $****P \leq 0.0001$.

Data, Materials, and Software Availability. All data are available in the main text and in *SI Appendix*. A portion of *Materials and Methods* is included in as *SI Appendix*.

ACKNOWLEDGMENTS. We thank Dr. Zorica Ristic for ensuring proper blinding to the treatment groups for investigators who conducted and assessed and/or quantified the results in the experiment of intranasal treatment poststroke. We thank Dr. Corina Berset and Dr. Paulin Jirkof, Department of Animal Welfare, University of Zurich, for their support in establishing anesthesia paradigms for intranasal application in rats and ETH Phenomics Center (EPIC) animal caretakers for their support during animal experimentation. Imaging was performed with the support of the Microscopy and Image Analysis Centre, University Zurich. Funding: This work was supported by the European Research Council advanced grant NOGORISE 294115 (to M.E.S.), a grant from the Swiss NSF (Grant #31003A-149315-1 to M.E.S.), and the EU Horizon 2020 grant Nr. 721098 – N2B-patch. Funders had no role in study design, data collection, analysis, decision to publish, or preparation of the manuscript.

Author affiliations: [a]Department of Health Sciences and Technology, Swiss Federal Institute of Technology-Zurich CH-8092, Zurich, Switzerland; [b]Institute for Regenerative Medicine, University of Zurich CH-8952, Zurich, Switzerland; [c]Institute of Neuropathology, University Hospital Zurich CH-8091, Zurich, Switzerland; [d]Interdisciplinary Center for Neuroscience, University of Heidelberg D-69120, Heidelberg, Germany; [e]Helmholtz Center Munich, Institute of Experimental Genetics D-85764, Neuherberg, Germany; [f]Brain Research Institute, University of Zurich CH-8057, Zurich, Switzerland; [g]Central Institute of Mental Health, University of Heidelberg D-68159, Heidelberg, Germany; and [h]Institute of Anatomy, Ludwig-Maximilians-University D-80336, Munich, Germany

Author contributions: D.C. and M.E.S. designed research; D.C.performed the overall experiments and data/evidence collection, except for mice experiments by M.I.S., H.S.,; D.C., M.I.S.,O.W.W., A.H., and K.L.S. carried out immunohistochemistry and microscopy; D.C. analyzed the overall data, except for mice studies by M.I.S., H.S., and brainstem analysis by A.H.; Y.A.B. assisted in experiments and data/evidence collection for the stroke study; A.-S.W. performed photothrombotic strokes and assistedr in neuroanatomical tracings; and D.C. and M.E.S. wrote the paper.

Competing interest statement: M.E.S. is the co-founder and president of the board of NovaGo Therapeutics AG. All other authors declare that they have no competing interests.

This article is a PNAS Direct Submission.

1. J. Ferrero *et al.*, First-in-human, double-blind, placebo-controlled, single-dose escalation study of aducanumab (BIIB037) in mild-to-moderate Alzheimer's disease. *Alzheimer's Dement. Transl. Res. Clin. Interv.* **2**, 169–176 (2016).
2. A. Ranger *et al.*, Anti-LINGO-1 has no detectable immunomodulatory effects in preclinical and phase 1 studies. *Neurol. Neuroimmunol. NeuroInflammation* **5**, 417 (2018).
3. P. O. Freskgård, E. Urich, Antibody therapies in CNS diseases. *Neuropharmacology* **120**, 38–55 (2017).
4. K. Kucher *et al.*, First-in-man intrathecal application of neurite growth-promoting anti-nogo- a antibodies in acute spinal cord injury. *Neurorehabil. Neural Repair* **32**, 578–589 (2018).
5. R. M. Lu *et al.*, Development of therapeutic antibodies for the treatment of diseases. *J. Biomed. Sci.* **27**, 1–30 (2020).
6. K. McFarthing *et al.*, Parkinson's disease drug therapies in the clinical trial pipeline: 2020. *J. Parkinsons. Dis.* **10**, 757–774 (2020).
7. I. St-Amour *et al.*, Brain bioavailability of human intravenous immunoglobulin and its transport through the murine blood-brain barrier. *J. Cereb. Blood Flow Metab.* **33**, 1983–1992 (2013).
8. B. Engelhardt, L. Sorokin, The blood-brain and the blood-cerebrospinal fluid barriers: Function and dysfunction. *Semin. Immunopathol.* **31**, 497–511 (2009).
9. W. Taal *et al.*, Single-agent bevacizumab or lomustine versus a combination of bevacizumab plus lomustine in patients with recurrent glioblastoma (BELOB trial): A randomised controlled phase 2 trial. *Lancet Oncol.* **15**, 943–953 (2014).
10. M. R. Gilbert *et al.*, A randomized trial of bevacizumab for newly diagnosed glioblastoma. *N. Engl. J. Med.* **370**, 699–708 (2014).
11. J. Sevigny *et al.*, The antibody aducanumab reduces Aβ plaques in Alzheimer's disease. *Nature* **537**, 50–56 (2016).
12. S. Salloway *et al.*, Amyloid positron emission tomography and cerebrospinal fluid results from a crenezumab anti-amyloid-beta antibody double-blind, placebo-controlled, randomized phase II study in mild-to-moderate Alzheimer's disease (BLAZE). *Alzheimer's Res. Ther.* **10**, 1–13 (2018).
13. D. R. Thal, U. Rüb, M. Orantes, H. Braak, Phases of Aβ-deposition in the human brain and its relevance for the development of AD. *Neurology* **58**, 1791–1800 (2002).
14. T. T. Hansel, H. Kropshofer, T. Singer, J. A. Mitchell, A. J. T. George, The safety and side effects of monoclonal antibodies. *Nat. Rev. Drug Discov.* **9**, 325–338 (2010).
15. Y. J. Yu *et al.*, Boosting brain uptake of a therapeutic antibody by reducing its affinity for a transcytosis target. *Sci. Transl. Med.* **3**, 1–9 (2011).

16. Y. J. Yu, R. J. Watts, Developing therapeutic antibodies for neurodegenerative disease. *Neurotherapeutics* **10**, 459–472 (2013).
17. Y. J. Y. Zuchero *et al.*, Discovery of novel blood-brain barrier targets to enhance brain uptake of therapeutic antibodies. *Neuron* **89**, 70–82 (2016).
18. J. S. Kanodia *et al.*, Prospective design of anti-transferrin receptor bispecific antibodies for optimal delivery into the human brain. *CPT Pharmacometrics Syst. Pharmacol.* **5**, 283–291 (2016).
19. J. F. Jordão *et al.*, Antibodies targeted to the brain with image-guided focused ultrasound reduces amyloid-β plaque load in the TgCRND8 mouse model of Alzheimer's disease. *PLoS One* **5**, 4–11 (2010).
20. H. M. Pappius, H. E. Savaki, C. Fieschi, S. I. Rapoport, L. Sokoloff, Osmotic opening of the blood-brain barrier and local cerebral glucose utilization. *Ann. Neurol.* **5**, 211–219 (1979).
21. C. C. Chen *et al.*, Targeted drug delivery with focused ultrasound-induced blood-brain barrier opening using acoustically-activated nanodroplets. *J. Control. Release* **172**, 795–804 (2013).
22. C. H. Fan *et al.*, Contrast-enhanced ultrasound imaging for the detection of focused ultrasound-induced blood-brain barrier opening. *Theranostics* **4**, 1014–1025 (2014).
23. S. I. Rapoport, D. S. Bachman, H. K. Thompson, Chronic effects of osmotic opening of the blood-brain barrier in the monkey. *Science (80-)* **176**, 1243–1245 (1972).
24. Z. I. Kovacsa *et al.*, Disrupting the blood-brain barrier by focused ultrasound induces sterile inflammation. *Proc. Natl. Acad. Sci. U.S.A.* **114**, E75–E84 (2017).
25. D. R. Groothuis, The blood-brain and blood-tumor barriers: A review of strategies for increasing drug delivery. *Neuro. Oncol.* **2**, 45–59 (2000).
26. P. Freund *et al.*, Nogo-A-specific antibody treatment enhances sprouting and functional recovery after cervical lesion in adult primates. *Nat. Med.* **12**, 790–792 (2006).
27. P. Calias, W. A. Banks, D. Begley, M. Scarpa, P. Dickson, Intrathecal delivery of protein therapeutics to the brain: A critical reassessment. *Pharmacol. Ther.* **144**, 114–122 (2014).
28. A. S. Wahl, Asynchronous therapy restores motor control by rewiring of the rat corticospinal tract after stroke. *Science (80-)* **344**, 1250–1255 (2014).
29. B. V. Ineichen *et al.*, Nogo-A antibodies enhance axonal repair and remyelination in neuro-inflammatory and demyelinating pathology. *Acta Neuropathol.* **134**, 423–440 (2017).
30. M. E. Pizzo *et al.*, Intrathecal antibody distribution in the rat brain: Surface diffusion, perivascular transport and osmotic enhancement of delivery. *J. Physiol.* **596**, 445–475 (2018).
31. J. J. Iliff *et al.*, Cerebral arterial pulsation drives paravascular CSF-Interstitial fluid exchange in the murine brain. *J. Neurosci.* **33**, 18190–18199 (2013).
32. E. N. T. P. Bakker *et al.*, Lymphatic clearance of the brain: Perivascular, paravascular and significance for neurodegenerative diseases. *Cell. Mol. Neurobiol.* **36**, 181–194 (2016).
33. R. G. Thorne, C. R. Emory, T. A. Ala, W. H. Frey, Quantitative analysis of the olfactory pathway for drug delivery to the brain. *Brain Res.* **692**, 278–282 (1995).
34. T. Sakane *et al.*, Direct drug transport from the rat nasal cavity to the cerebrospinal fluid: The relation to the molecular weight of drugs. *J. Pharm. Pharmacol.* **47**, 379–381 (1995).
35. R. G. Thorne, L. R. Hanson, T. M. Ross, D. Tung, W. H. Frey, Delivery of interferon-β to the monkey nervous system following intranasal administration. *Neuroscience* **152**, 785–797 (2008).
36. S. R. K. Vaka, S. M. Sammeta, L. B. Day, S. N. Murthy, Delivery of nerve growth factor to brain via intranasal administration and enhancement of brain uptake. *J. Pharm. Sci.* **98**, 3640–3646 (2009).
37. J. J. Lochhead, R. G. Thorne, Intranasal delivery of biologics to the central nervous system. *Adv. Drug Deliv. Rev.* **64**, 614–628 (2012).
38. M. B. Chauhan, N. B. Chauhan, Brain uptake of neurotherapeutics after intranasal versus intraperitoneal delivery in mice. *J. Neurol. Neurosurg.* **2**, 009 (2015).
39. S. Ladel *et al.*, Impact of glycosylation and species origin on the uptake and permeation of IgGs through the nasal airway mucosa. *Pharmaceutics* **12**, 1–24 (2020).
40. D. A. Simmons *et al.*, A small molecule TrkB ligand reduces motor impairment and neuropathology in R6/2 and BACHD mouse models of huntington's disease. *J. Neurosci.* **33**, 18712–18727 (2013).
41. J. Born *et al.*, Sniffing neuropeptides: A transnasal approach to the human brain. *Nat. Neurosci.* **5**, 514–516 (2002).
42. C. Benedict *et al.*, Intranasal insulin improves memory in humans: Superiority of insulin aspart. *Neuropsychopharmacology* **32**, 239–243 (2007).
43. D. P. O'Doherty, D. R. Bickerstaff, E. V. McCloskey, R. Atkins, N. A. Hamdy, A comparison of the acute effects of subcutaneous and intranasal calcitonin. *Clin. Sci. Lond* **78**, 215–259 (1990).
44. S. Cattepoel, M. Hanenberg, L. Kulic, R. M. Nitsch, Chronic intranasal treatment with an anti-Aβ30-42 scFv antibody ameliorates amyloid pathology in a transgenic mouse model of Alzheimer's disease. *PLoS One* **6**, 18296 (2011).
45. V. V. Kolobov, I. A. Zakharova, V. G. Fomina, V. Y. Gorbatov, T. V. Davydova, Effect of antibodies to glutamate on caspase-3 activity in brain structures of rats with experimental Alzheimer's disease. *Bull. Exp. Biol. Med.* **154**, 425–427 (2013).
46. R. G. Thorne, G. J. Pronk, V. Padmanabhan, W. H. Frey, Delivery of insulin-like growth factor-I to the rat brain and spinal cord along olfactory and trigeminal pathways following intranasal administration. *Neuroscience* **127**, 481–496 (2004).
47. J. J. Lochhead, D. J. Wolak, M. E. Pizzo, R. G. Thorne, Rapid transport within cerebral perivascular spaces underlies widespread tracer distribution in the brain after intranasal administration. *J. Perinatol.* **35**, 371–381 (2015).
48. N. N. Kumar *et al.*, Relative vascular permeability and vascularity across different regions of the rat nasal mucosa: Implications for nasal physiology and drug delivery. *Sci. Rep.* **6**, 1–14 (2016).
49. N. N. Kumar *et al.*, Delivery of immunoglobulin G antibodies to the rat nervous system following intranasal administration: Distribution, dose-response, and mechanisms of delivery. *J. Control. Release* **286**, 467–484 (2018).
50. S. Heidl, I. Ellinger, V. Niederberger, E. E. Waltl, R. Fuchs, Localization of the human neonatal Fc receptor (FcRn) in human nasal epithelium. *Protoplasma* **253**, 1557–1564 (2016).
51. S. S. Davis, L. Illum, Absorption enhancers for nasal drug delivery. *Clin. Pharmacokinet.* **42**, 1107–1128 (2003).
52. L. Ye, R. Zeng, Y. Bai, D. C. Roopenian, X. Zhu, Efficient mucosal vaccination mediated by the neonatal Fc receptor. *Nat. Biotechnol.* **29**, 158–165 (2011).
53. N. J. Abbott, M. E. Pizzo, J. E. Preston, D. Janigro, R. G. Thorne, The role of brain barriers in fluid movement in the CNS: is there a 'glymphatic' system?*Acta Neuropathol.* **135**, 387–407 (2018).
54. T. Oertle *et al.*, Nogo-A inhibits neurite outgrowth and cell spreading with three discrete regions. *J. Neurosci.* **23**, 5393–5406 (2003).
55. T. Liebscher *et al.*, Nogo-A antibody improves regeneration and locomotion of spinal cord-injured rats. *Ann. Neurol.* **58**, 706–719 (2005).
56. T. M. Markus *et al.*, Recovery and brain reorganization after stroke in adult and aged rats. *Ann. Neurol.* **58**, 950–953 (2005).
57. A. F. Wyssa *et al.*, Long-term motor cortical map changes following unilateral lesion of the hand representation in the motor cortex in macaque monkeys showing functional recovery of hand functions. *Restor. Neurol. Neurosci.* **31**, 733–760 (2013).
58. N. T. Lindau *et al.*, Rewiring of the corticospinal tract in the adult rat after unilateral stroke and anti-Nogo-A therapy. *Brain* **137**, 739–756 (2014).
59. A. S. Wahl *et al.*, Targeting Therapeutic Antibodies to the CNS: a Comparative Study of Intrathecal, Intravenous, and Subcutaneous Anti-Nogo A Antibody Treatment after Stroke in Rats. *Neurotherapeutics* **17**, 1153–1159 (2020).
60. A. B. Huber, O. Weinmann, C. Brösamle, T. Oertle, M. E. Schwab, Patterns of Nogo mRNA and Protein Expression in the Developing and Adult Rat and after CNS Lesions. *J. Neurosci.* **22**, 3553–3567 (2002).
61. Y. Noguchi, M. Kato, K. Ozeki, M. Ishigai, Pharmacokinetics of an intracerebroventricularly administered antibody in rats. *MAbs* **9**, 1210–1215 (2017).
62. I. Q. Whishaw, S. M. Pellis, The structure of skilled forelimb reaching in the rat: A proximally driven movement with a single distal rotatory component. *Behav. Brain Res.* **41**, 49–59 (1990).
63. W. J. Z'Graggen, G. A. S. Metz, G. L. Kartje, M. Thallmair, M. E. Schwab, Functional recovery and enhanced corticofugal plasticity after unilateral pyramidal tract lesion and blockade of myelin-associated neurite growth inhibitors in adult rats. *J. Neurosci.* **18**, 4744–4757 (1998).
64. W. B. J. Cafferty, S. M. Strittmatter, The Nogo-Nogo receptor pathway limits a spectrum of adult CNS axonal growth. *J. Neurosci.* **26**, 12242–12250 (2006).
65. G. A. Mihailoff, R. A. Burne, D. J. Woodward, Projections of the sensorimotor cortex to the basilar pontine nuclei in the rat: an autoradiographic study. *Brain Res.* **145**, 347–354 (1978).
66. R. J. Kosinski, E. J. Neafsey, A. J. Castro, A comparative topographical analysis of dorsal column nuclear and cerebral cortical projections to the basilar pontine gray in rats. *J. Comp. Neurol.* **244**, 163–173 (1986).
67. R. Wiesendanger, M. Wiesendanger, The corticopontine system in the rat. II. The projection pattern. *J. Comp. Neurol.* **208**, 227–238 (1982).
68. H. Lee *et al.*, Synaptic function for the Nogo-66 receptor NgR1: Regulation of dendritic spine morphology and activity-dependent synaptic strength. *J. Neurosci.* **28**, 2753–2765 (2008).
69. A. Delekate, M. Zagrebelsky, S. Kramer, M. E. Schwab, M. Korte, NogoA restricts synaptic plasticity in the adult hippocampus on a fast time scale. *Proc. Natl. Acad. Sci. U.S.A.* **108**, 2569–2574 (2011).
70. A. Kempf *et al.*, The sphingolipid receptor S1PR2 is a receptor for Nogo-A repressing synaptic plasticity. *PLoS Biol.* **12**, e1001763 (2014).
71. L. M. Craveiro *et al.*, Neutralization of the membrane protein Nogo-A enhances growth and reactive sprouting in established organotypic hippocampal slice cultures. *Eur. J. Neurosci.* **28**, 1808–1824 (2008).
72. M. Zagrebelsky, R. Schweigreiter, C. E. Bandtlow, M. E. Schwab, M. Korte, Nogo-A stabilizes the architecture of hippocampal neurons. *J. Neurosci.* **30**, 13220–13234 (2010).
73. A. Zemmar *et al.*, Neutralization of Nogo-A enhances synaptic plasticity in the rodent motor cortex and improves motor learning in vivo. *J. Neurosci.* **34**, 8685–8698 (2014).
74. X. Wang *et al.*, Localization of Nogo-A and Nogo-66 receptor proteins at sites of axon-myelin and synaptic contact. *J. Neurosci.* **22**, 5505–5515 (2002).
75. C. Rolando *et al.*, Distinct roles of Nogo-A and nogo receptor 1 in the homeostatic regulation of adult neural stem cell function and neuroblast migration. *J. Neurosci.* **32**, 17788–17799 (2012).
76. M. Brus-Ramer, J. B. Carmel, S. Chakrabarty, J. H. Martin, Electrical stimulation of spared corticospinal axons augments connections with ipsilateral spinal motor circuits after injury. *J. Neurosci.* **27**, 13793–13801 (2007).
77. J. B. Carmel, L. J. Berrol, M. Brus-Ramer, J. H. Martin, Chronic electrical stimulation of the intact corticospinal system after unilateral injury restores skilled locomotor control and promotes spinal axon outgrowth. *J. Neurosci.* **30**, 10918–10926 (2010).
78. M. L. Starkey, C. Bleul, I. C. Maier, M. E. Schwab, Rehabilitative training following unilateral pyramidotomy in adult rats improves forelimb function in a non-task-specific way. *Exp. Neurol.* **232**, 81–89 (2011).
79. I. C. Maier *et al.*, Constraint-induced movement therapy in the adult rat after unilateral corticospinal tract injury. *J. Neurosci.* **28**, 9386–9403 (2008).
80. M. A. Deli, Potential use of tight junction modulators to reversibly open membranous barriers and improve drug delivery. *Biochim. Biophys. Acta Biomembr.* **1788**, 892–910 (2009).
81. L. Illum, Transport of drugs from the nasal cavity to the central nervous system. *Eur. J. Pharm. Sci.* **11**, 1–18 (2000).
82. R. D. Broadwell, B. J. Balin, Endocytic and exocytic pathways of the neuronal secretory process and trans synaptic transfer of wheat germ agglutinin-horseradish peroxidase in vivo. *J. Comp. Neurol.* **242**, 632–650 (1985).
83. S. Craft *et al.*, Intranasal insulin therapy for Alzheimer disease and amnestic mild cognitive impairment: a pilot clinical trial. *Arch. Neurol.* **69**, 29–38 (2012).
84. A. Hamidovic *et al.*, Reduction of smoking urges with intranasal insulin: a randomized, crossover, placebo-controlled clinical trial. *Mol. Psychiatry* **22**, 1413–1421 (2017).
85. M. L. Starkey *et al.*, Back seat driving: Hindlimb corticospinal neurons assume forelimb control following ischaemic stroke. *Brain* **135**, 3265–3281 (2012).